

# A numerical investigation of friction stir welding parameters in joining dissimilar aluminium alloys using finite element method

Moradi, M., Shaikh Mohammad Meiabadi, M. S. & Demers, V.

**Author post-print (accepted) deposited by Coventry University's Repository**

**Original citation & hyperlink:**

Moradi, M, Shaikh Mohammad Meiabadi, MS & Demers , V 2021, 'A numerical investigation of friction stir welding parameters in joining dissimilar aluminium alloys using finite element method', International Journal of Manufacturing Research, vol. 16, no. 1, pp. 32 -51.  
<https://dx.doi.org/10.1504/IJMR.2021.10028488>

DOI 10.1504/IJMR.2021.10028488

ISSN 1750-0591

ESSN 1750-0605

Publisher: Inderscience

**Copyright © and Moral Rights are retained by the author(s) and/ or other copyright owners. A copy can be downloaded for personal non-commercial research or study, without prior permission or charge. This item cannot be reproduced or quoted extensively from without first obtaining permission in writing from the copyright holder(s). The content must not be changed in any way or sold commercially in any format or medium without the formal permission of the copyright holders.**

**This document is the author's post-print version, incorporating any revisions agreed during the peer-review process. Some differences between the published version and this version may remain and you are advised to consult the published version if you wish to cite from it.**

# **A Numerical Investigation of Friction Stir Welding Parameters in Joining Dissimilar Aluminum Alloys Using Finite Element Method**

Mahmoud Moradi <sup>1\*</sup>, M.Saleh Meiabadi<sup>2</sup>, Vincent Demers<sup>2</sup>

1- Department of Mechanical Engineering, Faculty of Engineering, Malayer University, Malayer, Iran.

2-Department of Mechanical Engineering, École de technologie supérieure, Canada  
1100 Notre-Dame West, Montreal, QC, H3C 1K3, Canada.

## **Abstract**

Friction stir welding is a relatively new solid-state welding process which has several superiorities over generic welding methods. In this study, aluminum alloys (AA5083-O and AA6061-T6) are selected to investigate effects of three welding variables namely tool rotation speed, tool traverse speed, and tool diameter on temperature distribution, weld width, weld depth, and heat affected zone width using finite element method. The Johnson-Cook plasticity model is implemented into Abaqus software to simulate the material plastic deformation occurring during welding process. The results demonstrated that increasing rotational speed and tool diameter lead in an increase in material temperature. Increasing traverse speed resulted in lower temperature distribution. Temperature distribution, as well as the size and shape of welding areas, are also different due to different mechanical and thermal properties. The wider heat affected zone predicted for the AA6061-T6 can be explained by its higher thermal conductivity and lower specific heat.

**Keywords:** Friction stir welding, Aluminum alloys, Simulation, Finite element method

## 1-Introduction

Aluminum alloys have been used in many industries, namely aerospace, shipbuilding, trains, automotive, and many other sectors due to their heat transfer properties, high strength to weight ratio, and high ductility. AA5083-O is known for its exceptional performance in aggressive (corrosion) environment. AA 5083 has high resistance to corrosion [1] and is used in marine applications [2]. It has a low density and good thermal conductivity shared by all aluminum alloys. Alloy 5083 also exhibits exceptional strength after welding [3]. AA6061-T6 properties include its excellent structural strength, good toughness, good finishing characteristics, excellent anodizing properties, making it an adequate choice in several industries [4]. Joining aluminum alloys by traditional fusion welding methods such as gas tungsten arc welding (GTAW) or gas metal arc welding (GMAW) generally required high heat input for the formation of the fusion pool which is detrimental for the mechanical properties of the assemblies due to the formation of defects (porosity, lack of fusion, hot cracking), wide heat affected zone (HAZ), and heterogeneous residual stress. Recently, the joining methods of aluminum alloys have been increasingly developed [5, 6].

Friction stir welding (FSW) is a solid-state joining method which necessitates lower heat input resulting in a reduction of volumetric defects typically found in the conventional liquid-state welding techniques [7, 8]. It is an energy efficient, environmentally friendly, and versatile joining process [7]. The solid-phase of the welding operation produces low distortion, good appearance welds which is also cost-effective to join most aluminum alloys [8].

Many researchers have investigated the FSW process using experimental and numerical approaches. Raikoty et al. analyzed high-speed FSW of Aluminium 6061-T6 by a 3D numerical model. The temperature distributions in the welding parts were predicted in terms of traverse speed. The experimental results of surface temperatures were lower than the results of the computational scheme. The appropriate range of spindle translation velocity to obtain a sound weld was 125 mm/min and 250 mm/min [9].

Jamshidi et al. investigated numerically and experimentally similar and dissimilar FSW of AA6061-T6 and AA5086-O materials. The experimental and numerical results indicated that the peak temperature during FSW of similar AA6061 joint was maximum in comparison with other joints at the same processing parameters. Characterization of mechanical properties and the evolution of microstructures showed different strengthening mechanisms in the materials. Results indicated the hardness variation in the similar AA5086-O joints was influenced by recrystallization and generation of fine grains in weld nugget. However, variations of hardness in the similar AA6061 joint and the dissimilar joint relied on subsequent aging phenomenon [10].

Dubourg et al. conducted several feasibility tests to join 1.5mm Aluminium 7075-T6 stringers to 2.3mm Aluminium 2024-T3 skins by FSW. The effects of travel speed and rotation speed on mechanical and metallurgical properties of materials were studied. Moreover, the optimal joint configuration was determined by changing the advancing and retreating side locations. Results showed an increasing travel speed and decreasing rotational speed had an influence on the reduction of the hooking size and top plate thinning but could not eliminate them. Double pass welds by overlapping the advancing sides were found to be the best joint configuration for FSW lap joints [11]. Kumbhar et al. aimed to comprehensively examine microstructural development in the FSW of AA5052. The researchers metallurgically investigated base material, nugget, advancing side, and retreating side in the welding region. Results indicated that microstructure development was clearly asymmetric with different microstructural indices at different regions. The nugget region, retreating side, and advancing side were found to be the strongest regions respectively. They suggested lower

rotational speed resulted in higher tensile strength and elongation than higher rotational speed [12]. Ji et al. utilized a finite volume model to numerically simulate FSW to study effects of tool geometry on the plastic flow of material. The results of numerical simulation showed that the flow velocity of the material decreases with increasing the distance away from the weldment surface or the rotational axis of pin. The authors confirmed that shoulder and pin geometries could be influential in improving material flow during FSW and weld quality [13]. Optimum friction stir welding parameters were obtained by Sadeesh et al. to join dissimilar sheets of AA 5052-H32 and AA 5754-H22 using a statistical approach. The effects of rotational speed and traverse speed on microstructural, hardness, and tensile properties were studied using five different tool designs. The microstructural properties indicated that the material placed on the advancing side has a major influence on the nugget region. The low hardness zone was identified in the HAZ corresponding to the failure location during the tensile studies [14]. Kesharwani et al. optimized process parameters affecting ultimate strength and elongation of the dissimilar weld between AA5052-H32 and AA5754-H22 thin sheets in tailored friction stir butt welding by Taguchi grey method. The rotational tool speed, translational worktable speed, tool shoulder diameter, and tool pin geometry have been considered as input factors. The uniaxial tensile tests were conducted to determine mechanical performances of these joints. The analysis of variance results revealed that rotational tool plays a major role in the mechanical characteristics of the joints [15]. Cho et al. carried out several experiments for friction stir welding of A5083 and A6082 aluminum alloys by a concave shoulder and a threaded conical pin. The temperature profile near heat affected zone was measured by thermocouples and microstructural features of the samples were investigated by electron backscatter diffraction (EBSD). The temperature profile demonstrated similar peak temperatures in the A5083 and A6082 alloys [16]. Dialami et al. proposed a coupling strategy for the simulation of the temperature histories and consequently residual stresses in the FSW of 304 L stainless steel. At the local level the process zone nearby the pin tool was analyzed and at the global level the entire structure was simulated. The power heat input was computed in the local level analysis to be used as an input in the global level analysis. The viscous dissipation and friction were considered in the computation of the total heat power. The authors concluded that the proposed method could be used to more accurately calculate residual stresses [17].

Iordache et al. simulated FSW using coupled Eulerian-Lagrangian formulation by Abaqus/Explicit software. Temperatures at 6 points across of a butt joint between two plates were measured by thermocouples during FSW process and compared with numerical results. Numerical results corresponded to experimental results very well confirming that the numerical model was validated [18]. Paulo et al. developed a numerical model including a softening model which aimed at prediction of temperature and hardness distribution in the AA2024-T3 plates. The proposed model was validated using experimental data obtained by hardness measurement of the plate cross-section. The authors claimed that the proposed model offered acceptable results for prediction of softening in HAZ area [19]. Moosun and Jung simulated FSW of magnesium alloy AZ31 by Fluent software. In the numerical analysis, the magnesium alloy was innovatively considered as a non-Newtonian viscous fluid. The rotational speed, feed speed of the base material, and shape of the tool were regarded as process parameters to investigate temperature history. Experimental measurements showed that temperature profiles agreed well with simulation results [20]. Chen et al. investigated effects of pin threads on material flow during FSW of an Al-Mg-Zn alloy by computational fluid dynamics (CFD). The numerical simulation was validated by experimental measurement of temperature at 8 different points. The results indicated that the pin thread contributed into enhanced strain rate, trap material in the high-velocity zone, and a vertical pressure gradient

[21]. Costa et al. conducted a parametric study on distortion and residual stresses in FSW of AA5754-H22 aluminum plates by FEM. It was also seen by experimental investigation that dimensional features of the plates mainly plate width affects both the distortion magnitude and mode, as well as the longitudinal residual stresses. Results indicated that although welding speed had an important impact on distortion, tool stirring action had no effect on it [22].

The FSW of dissimilar materials is a challenging process which results in different mechanical and metallurgical properties in the joining materials. Though large amount of research have been conducted on numerical simulation of FSW to study effects of process parameters on mechanical properties, metallurgical properties, and defects of dissimilar welds, there is little in the literature about dimensional characterization of the dissimilar joint using finite element method (FEM). The dimensional characterization of different welding areas is conducted in the present research using predicted temperature distribution and element size. Moreover, it can be costly and time-consuming to study FSW process experimentally, while the experimental investigations may be inaccurate due to the difficulty of reproducing the production conditions [23]. The FEM offers the opportunity to inspect different aspects of the manufacturing process without the use of a real-scale physical prototype [24]. Therefore, in this study, a FE model is developed to analyze the FSW of AA6061-T6 and AA5083-O alloys. The Arbitrary Lagrangian-Eulerian (ALE) description is utilized to maintain mesh distortion under control and the mass scaling method is used to reduce computation time. The purpose of the paper is to examine the effects of processing parameters and tool diameter on the temperature distribution and the size and shape of different welding areas using FE modeling of friction stir welding for two aluminum types.

## 2- Development of FE model

A 3D transient explicit FE method is used to simulate the coupled and highly-nonlinear thermomechanical phenomena occurring during friction stir welding. The thermomechanical simulation is a significant method to determine the size and shape of different welding areas. Fig. 1a demonstrates the localized zone of welding in the geometrical model using dashed line. Fig. 1b depicts welding speed of tool is defined by inflow and outflow material velocities over the Eulerian domain boundaries [25].

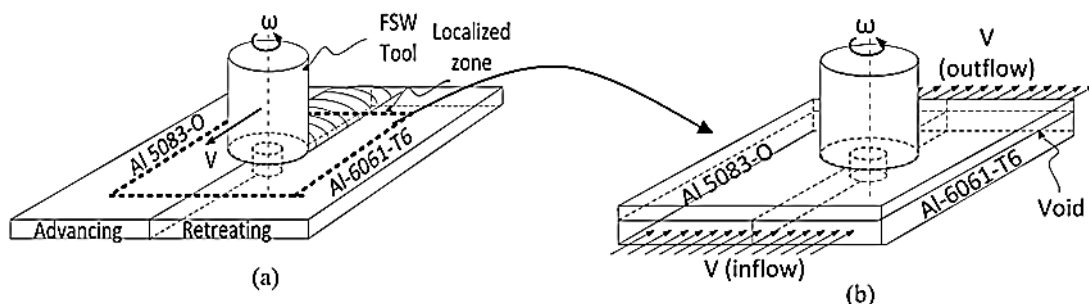


Fig. 1 (a) Dissimilar welding of AA6061-T6 and AA5083-O using butt joint configuration; (b) Applying welding speed by inflow and outflow velocities [25]

Simulation of FSW process is modeled using a rectangular plate ( $80 \times 60 \times 6$  mm), the material properties are defined to 5 mm part thickness. A one-millimeter remained thickness is modeled so that the flow of material that occurs during welding at the top of the work piece is visible. In the FE model, AA6061-T6 and AA5083-O parts are meshed using coupled temperature-displacement elements to conduct thermal/mechanical analysis which is a nonlinear simultaneous solution of temperature and displacement for thermomechanical

problems. The temperature dependent mechanical and physical properties of base materials are obtained from the literature [26, 27]. Table 1 and 2 show temperature-dependent properties of AA5083-O and AA6061-T6, accordingly. The accuracy of temperature distribution and stress field predictions by FE model is affected by the proper definition of material properties. The thermal properties of AA5083-O and AA6061-T6 are illustrated in Fig 2 and Fig 3 respectively are obtained from the literature [28, 29]. Finally, the harder alloy (AA6061-T6) is located at the retreating side, while the softer alloy (AA5083-O) is positioned in the advancing side.

**Table 1 Temperature-dependent properties for Al 5083-O [26]**

Temperature (°C)	25	100	150	200	250	300	400	500
Yield strength (MPa)	176	176	176	176	176	176	176	176
Young’s modulus (GPa)	72	70	67	62	42	41	28	15
Thermal exp.( $\mu$ m/m K)	24.2	24.2	24.2	24.2	24.2	24.2	24.2	24.2
Density (kg/m3)	2659	2638	2632	2625	2617	2609	2584	2561

**Table 2 Temperature-dependent properties for Al 6061-T6 [27]**

Temperature (°C)	25	37.8	93.3	148.9	204.4	260	315.6	371.1	426.7
Yield strength (MPa)	276	274.4	264.6	248.2	218.6	159.7	66.2	34.5	17.9
Young’s modulus (GPa)	68.9	68.54	66.19	63.09	59.16	53.99	47.48	40.34	31.72
Thermal exp.( $\mu$ m/m K)	22	23.45	24.61	25.67	26.6	27.56	28.53	29.57	30.71
Density (kg/m3)	2,700	2,685	2,685	2,667	2,657	2,657	2,630	2,620	2,602

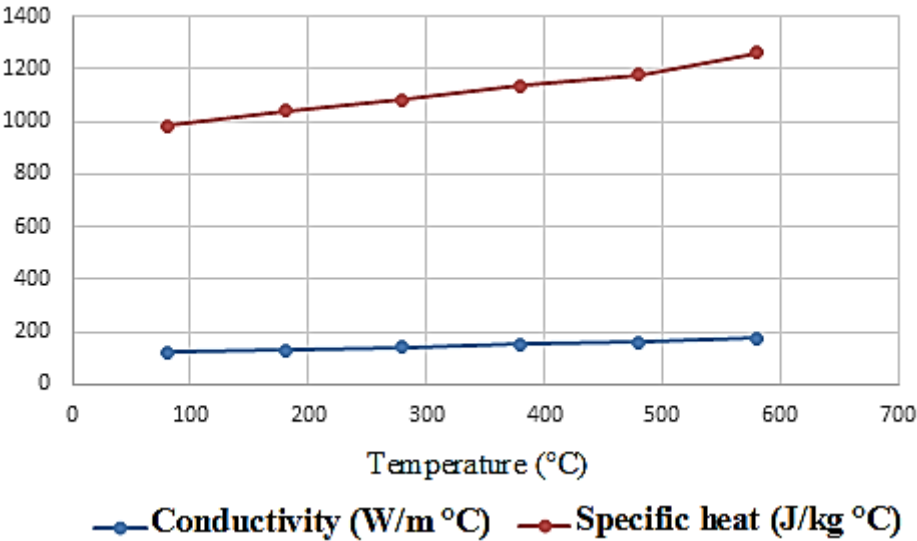


**Fig 2. Thermal properties of Aluminum Alloy 5083-O**

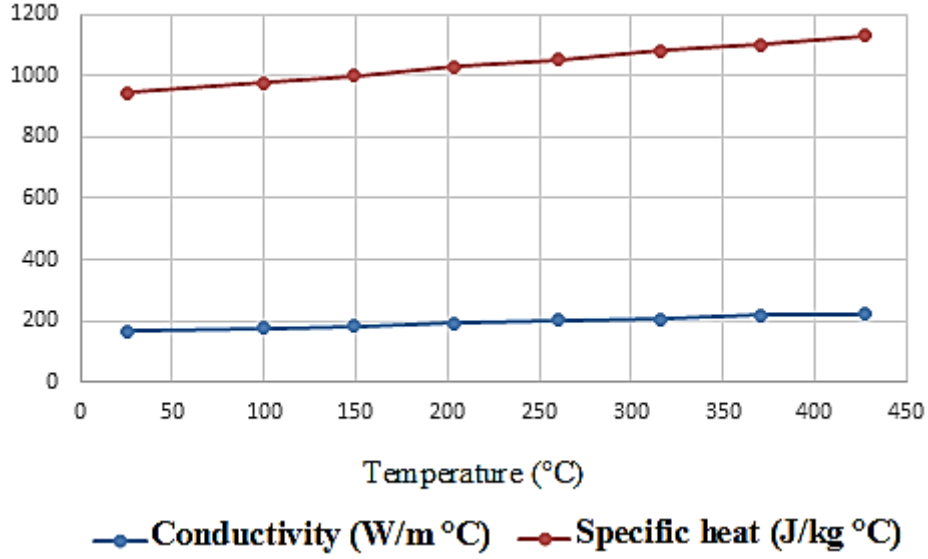


Fig 3. Thermal properties of Aluminum Alloy 6061-T6

Johnson-Cook plasticity model described by Equation (1) is used to predict the material's plastic behavior [30, 31]. This description is widely used to implement the strain-stress behavior in the plastic range and consider the separated effects of strain hardening, strain-rate, and thermal softening [32]. The Johnson-Cook constants of Al-6061-T6 and Al 5083-O are reported in Table 3.

Table 3 The Johnson-Cook input constants [26]

Material	A [MPa]	B [MPa]	C	n	m	$T_{room}$ [k]	$T_{melt}$ [k]
Al-6061-T6	324	114	0.002	0.42	1.34	297	856
Al-5083-O	170	425	0.0335	0.42	1.225	297	913

$$\sigma_y = (A + B\bar{\epsilon}^{p^n}) (1 + c \ln \dot{\epsilon}^*) (1 - T^{*m}) \quad (1)$$

where  $A$ ,  $B$ ,  $C$ ,  $n$ , and  $m$  are user defined input constants,  $\bar{\epsilon}^p$  is the effective plastic strain, and:

$$\dot{\epsilon}^* = \frac{\dot{\bar{\epsilon}}^p}{\dot{\epsilon}_0} \quad (2)$$

is the effective plastic strain rate for  $\dot{\epsilon}_0 = 1 \text{ s}^{-1}$ , and:

$$T^* = \frac{T - T_{room}}{T_{melt} - T_{room}} \quad (3)$$

$T$  is the temperature,  $T_{room}$  is the room temperature, and  $T_{melt}$  is the melting point of the material).

The part is meshed by 93025 nodes and 86400 Eulerian elements (Ec 3D 8RT). The tool is meshed by 2412 nodes and 2416 R3D4 square elements and also modeled as discrete rigid due to the higher strength of the tool compared to aluminum. Figure 3 presents the FSW tool dimensions and the 3D model of the tool where the smaller diameter of the pin is considered

as the tool diameter in the analysis. The friction coefficient is set at 0.8 and Coulomb's friction model is used [25]. In the present model, the lower and lateral surfaces of the workpiece are positioned in the direction perpendicular to the surfaces. The tool moves vertically at the step of tilting the workpiece and rotationally around its axis. The isothermal tool is considered and its degree of thermal freedom is bound. For the workpiece, the initial temperature is considered 20 (°C) while its temperature evolution during welding is investigated. The sensitivity of the FE model is evaluated by the convergence test for sizing mesh to explore the sensitivity of the model predictions towards the size of elements

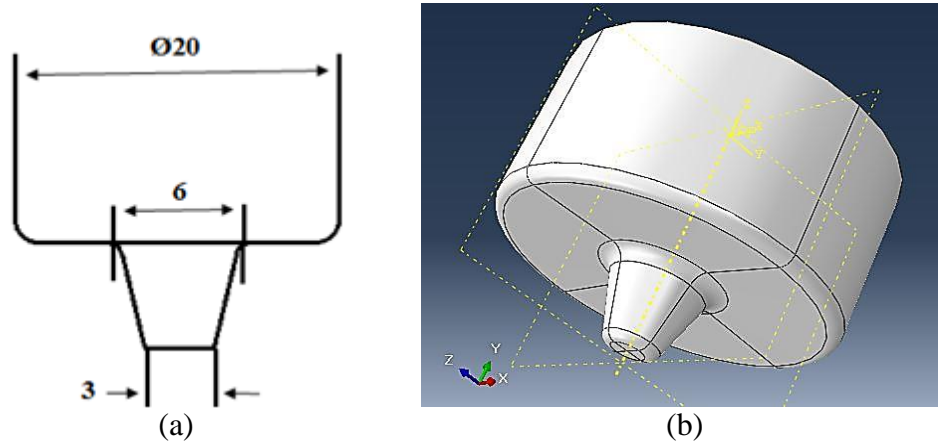
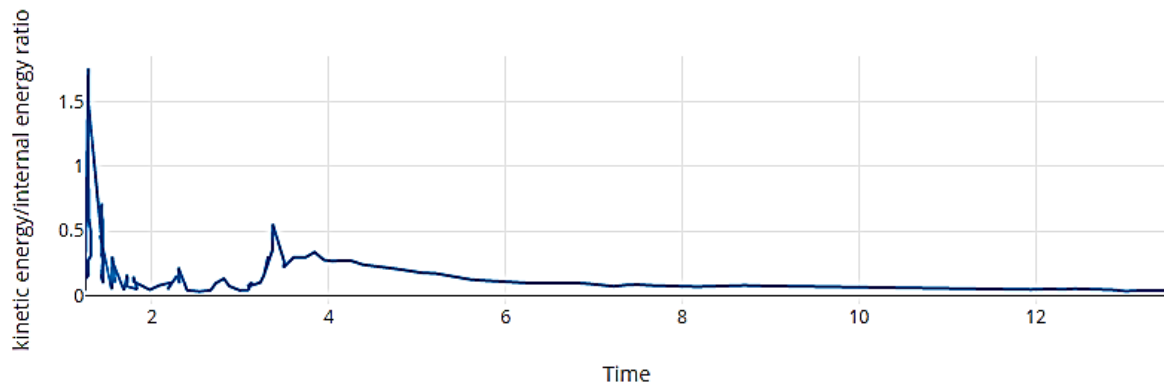


Fig 3. (a) FSW tool geometrical dimensions (b) 3D representation of the tool (3 mm diameter of the pin is considered as the tool diameter)

## 2-1 Computational Efficiency

Due to drawbacks of the both Lagrangian and Eulerian approaches, a technique is developed to cope with difficulties of the numerical simulation of engineering problems which is known as the Arbitrary Lagrangian-Eulerian (ALE) description [30]. ALE mesh technique is adopted to avoid mesh distortion during the analysis by automatic re-meshing and freedom of the mesh to move independently of the material. The ALE technique amends the accuracy of results, nonetheless generally increases the computation time. In the current analysis, the mass scaling method is used to reduce the computation time because the variation of the material density does not change the generated heat from friction and plastic deformation. To assess the efficiency of mass-scaling method, the ratio of the kinematic energy and the internal energy must be less than 10% to reveal that the simulation is still a quasi-static problem [26]. The ratio of kinematic energy and the internal energy is plotted in Fig 4 which confirms that the FSW process is quasi-static.



**Fig 4. The kinetic energy/internal energy ratio of the system**

## 2-2 Verification of the FE model

The FE model is verified by comparing the predicted maximum temperature at 10 mm from the center of the weldline at both sides with the experimental data obtained from the reference article at the same condition [25]. Results summarized in Table 4 show that there is a suitable agreement between experimental data and simulation results (i.e., less than 14% of error). Therefore the FE is validated to study effects of process parameters.

**Table 4 Comparison between experimental and FE model results in the maximum temperatures at 10 mm from the centerline of the weld**

Input parameters			Type of results	Maximum temperature (°C)	
Rotational speed(rpm)	Traverse Speed(mm/s)	Tool diameter		Advancing side AA5083-O	Retreating side AA6061-T6
900	2.5	3	Experimental	646	621
			FE model	729	707
			Error	-12.8%	-13.8%

## 3- Simulation Set-up

Three parameters of tool rotational speed, tool traverse speed, and tool diameter are considered as input parameters while weld width, weld depth, and HAZ width as output parameters. In the present research the weld nugget or dynamically recrystallized zone (DXZ) and the thermomechanically affected zone (TMAZ), are considered as weld width. The effect of each input parameter is investigated by keeping two input parameters constant and varying the third one while the output parameters are recorded and presented in Table 5 in term of weld width, weld depth, and HAZ width for each side of the joints (i.e., for each material). Test 1 is the reference conditions to better understand the impact of each input parameters. The rotational speed, the traverse speed, and the diameter of the tool are changed during the experiments 1-4, 5-7, and 8-10, respectively.

**Table 5 Levels of input parameters and output responses in the experiments**

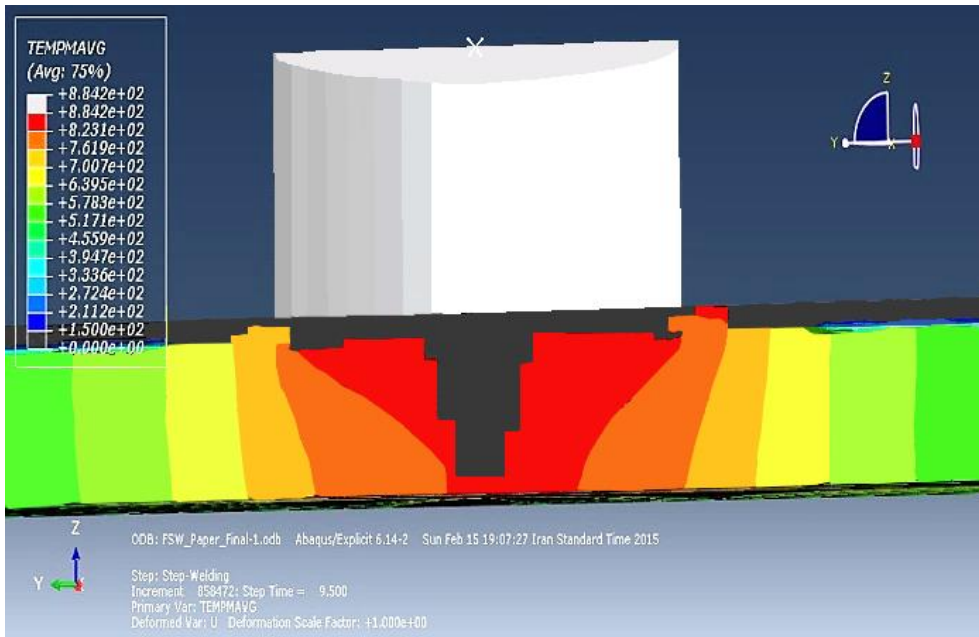
No	Input Parameters			Output responses					
	Rotation speed [rpm]	Traverse speed [mm/s]	Tool diameter [mm]	Weld Width (mm)		Weld Depth (mm)		HAZ Width	
				WW 6061-T6	WW 5083-O	H 6061-T6	H 5083-O	HW 6061-T6	HW 5083-O
1	940	2.5	3.5	10	9.333	6	6	12	10
2	740	2.5	3.5	8	9.2	6	2	10	9.667
3	1040	2.5	3.5	10	9.333	6	6	11.466	10
4	1140	2.5	3.5	8.7	7.333	6	6	10.666	9.466
5	940	1.5	3.5	10	8	5	1.75	10.8	9.466
6	940	3.5	3.5	8.6667	8.666	5.75	2.25	10.133	9.466
7	940	4.5	3.5	9.3333	8.666	6	6	10.2	9.866
8	940	2.5	2	8	7.466	6	3.25	9.933	9.466
9	940	2.5	2.5	8.1333	8	6	6	12	9.533
10	940	2.5	3	9.333	9.466	6	6	12.666	10

## 4-Results and discussion

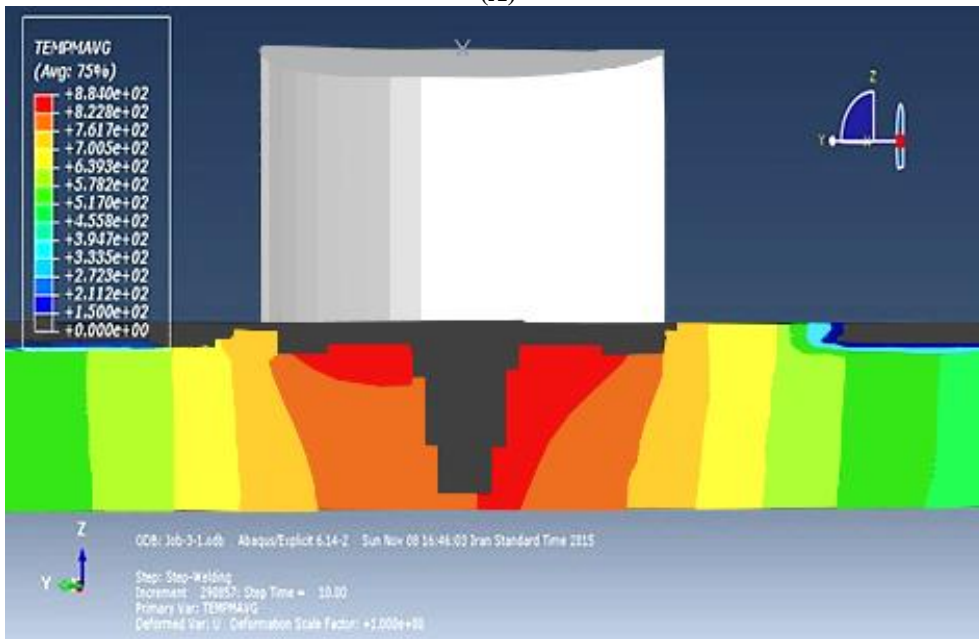
The effects of the three main input parameters of the rotational speed, traverse speed, and tool diameter on the weld width, weld depth, and HAZ in both sides are analyzed. The frictional heating and plastic deformation are the main reasons for generation of heat during FSW process. The generated heat disperses in the parts by conduction, while free convection and radiation dissipate some parts of the generated heat to surroundings [21]. The heat generation is strongly influenced by the motion of the welding tool which includes rotational and transverse speeds [33]. The dimensions of the weld width, weld depth, and HAZ are measured based on the size of the elements.

### 4-1 Effects of rotational speed

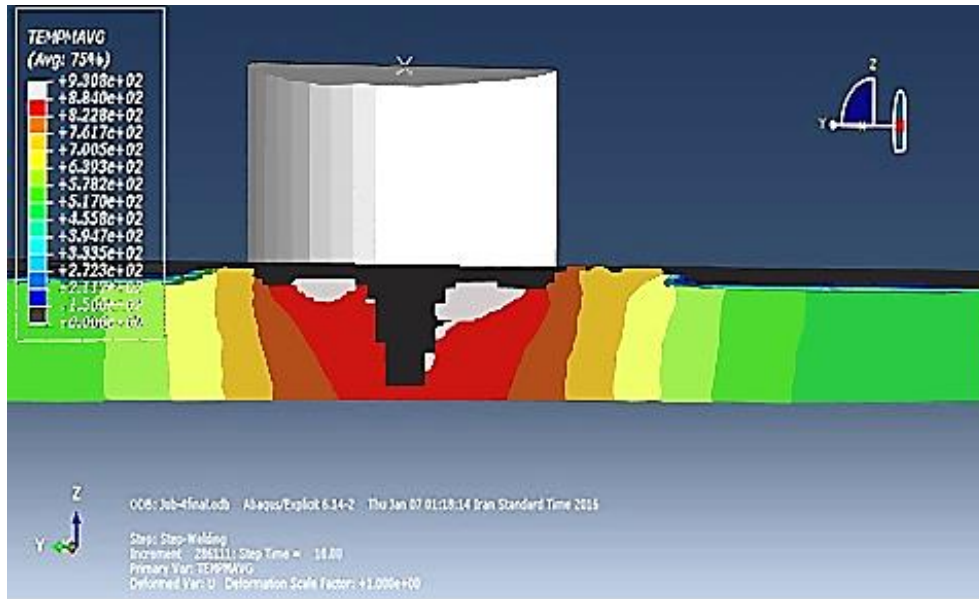
Figure 5 shows simulated temperature distributions across the welding zone at different rotational speeds indicating that an increase in the rotational speed produces, as expected, an increase in temperature within the material. As a matter of fact, this increase in temperature distribution at higher rotational speed can be explained by increasing strain rates and thus plastic deformations. Figure 5(D) illustrates the maximum operating temperature of 1037 K obtained at the maximum rotational speed of 1140 rpm which is the undesirable condition for solid-state FSW process. Figure 6 presents the evolution of weld width according to the rotational speed for the two aluminum alloys. At the rotating speed of 740 rpm, the weld width of AA5083-O is larger, whereas it becomes narrower than the AA6061-T6 weld joint when rotating speeds are increased. Figure 7 shows effects of rotational speed on the weld depth at different rotational speeds where full penetration is seen for both aluminum alloys at all rotational speed except for AA5083-O at a speed of 740 rpm probably due to low heat input in this case. Figure 8 shows the effects of rotational speed on HAZ width for the two aluminum alloys where the zones affected by heat of the AA6061-T6 seem to be always larger than that obtained for AA5083-O.



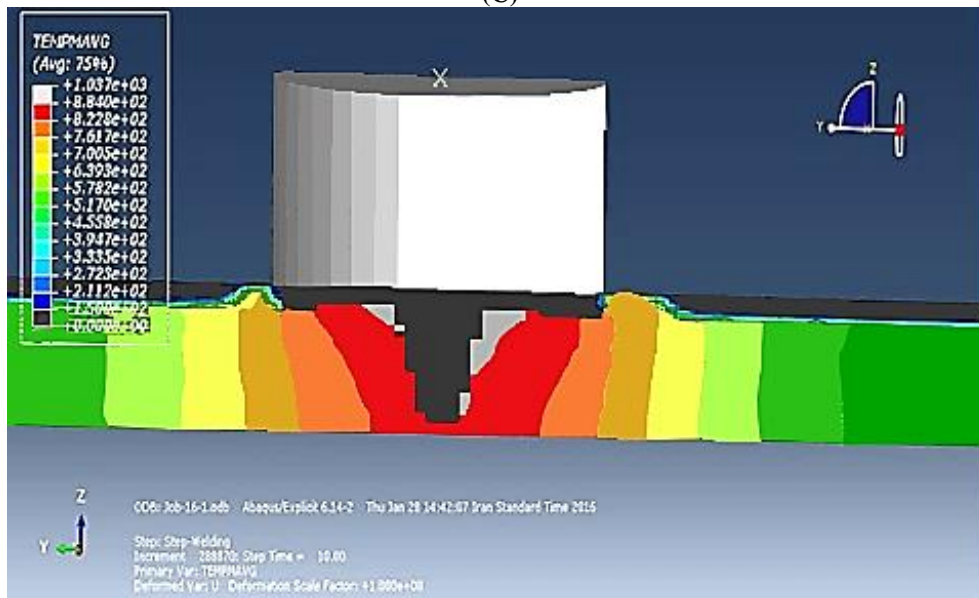
(A)



(B)



(C)



(D)

Fig 5 Effects of rotational speed on the weld width, weld depth, and HAZ width for rotation speeds of A) 940 rpm, B) 740 rpm, C) 1040 rpm, and D) 1140 rpm

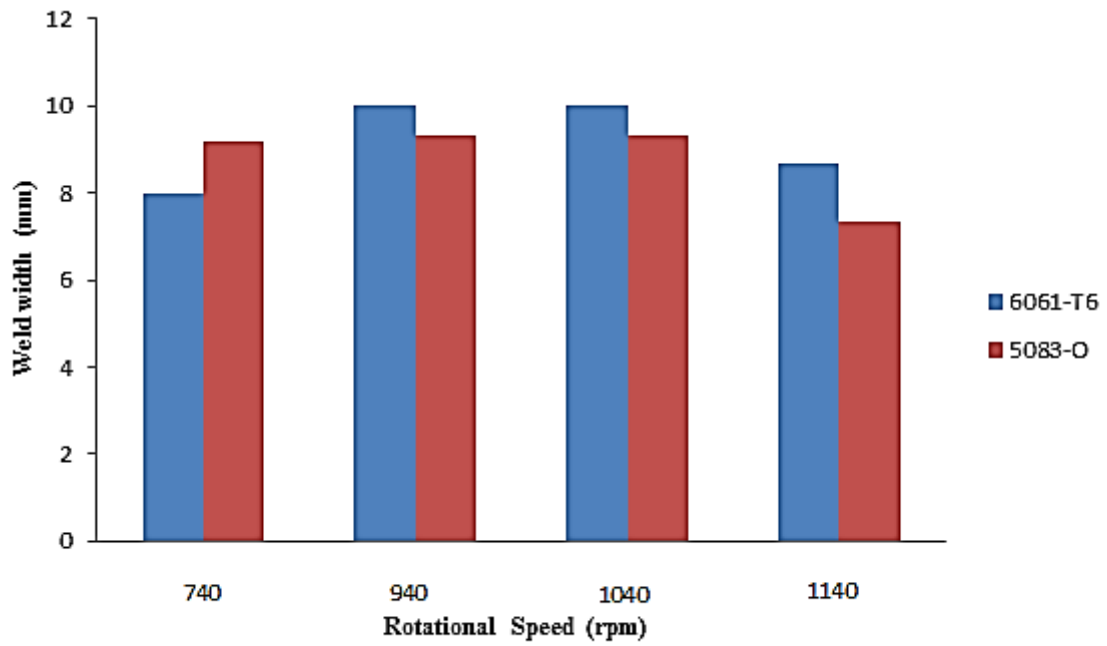


Fig. 6 - Effects of rotational speed on the weld width for the two aluminum alloys.

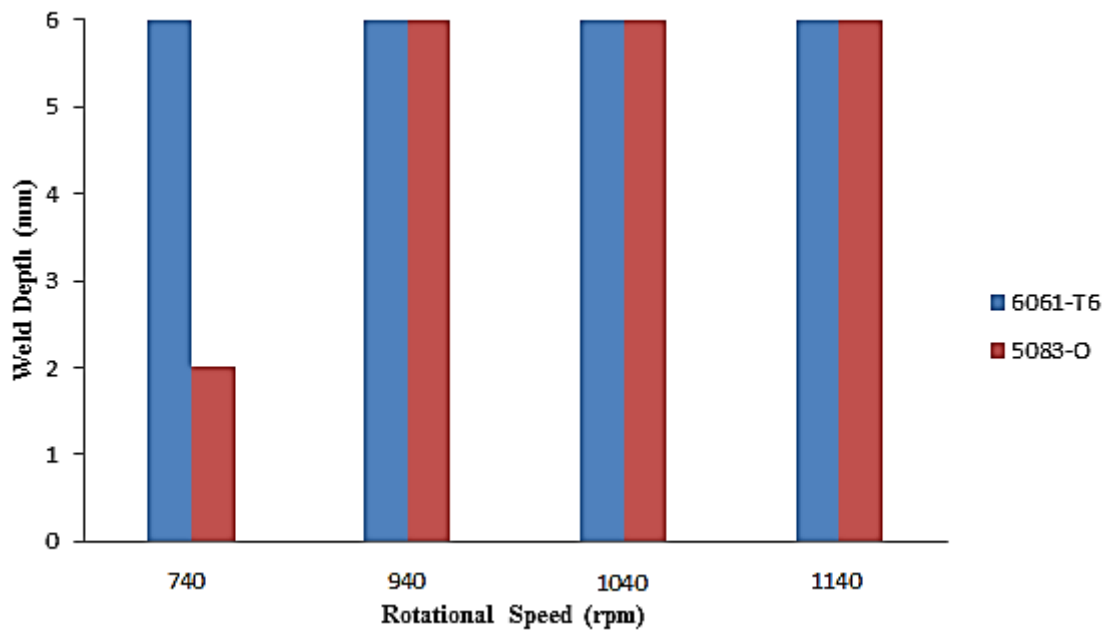


Fig 7. Effects of rotational speed on the weld depth for the two aluminum alloys.

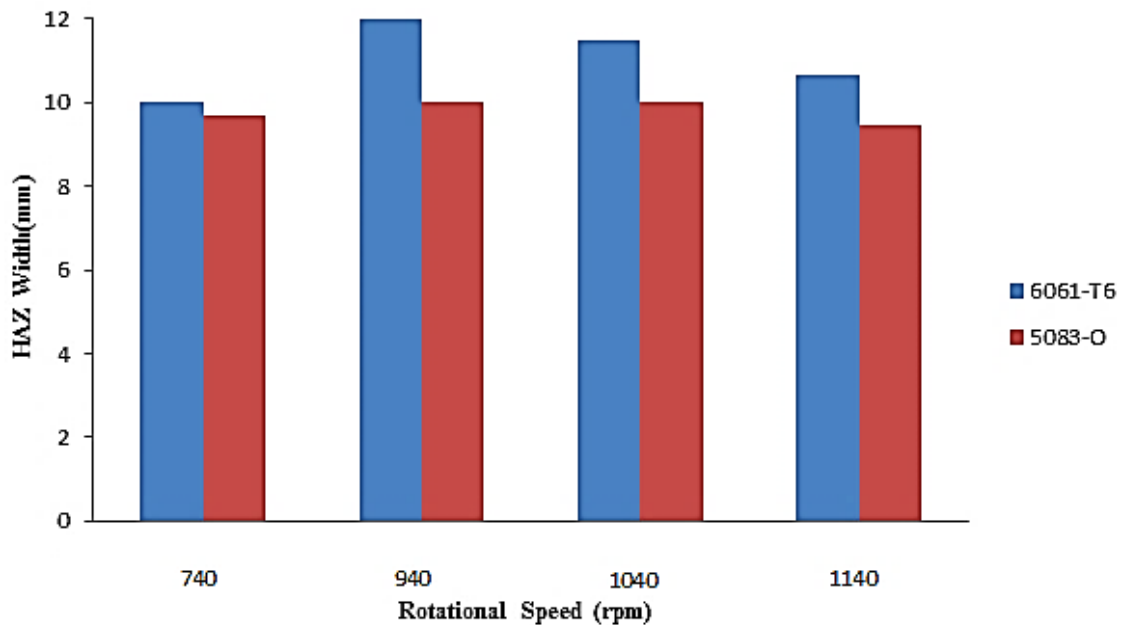
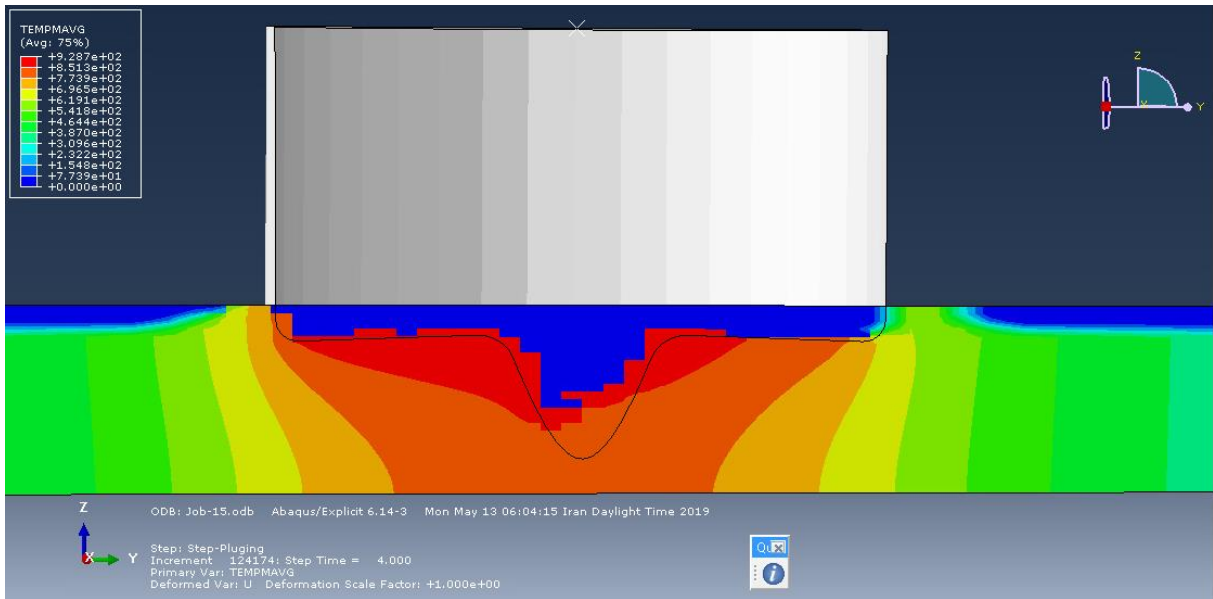


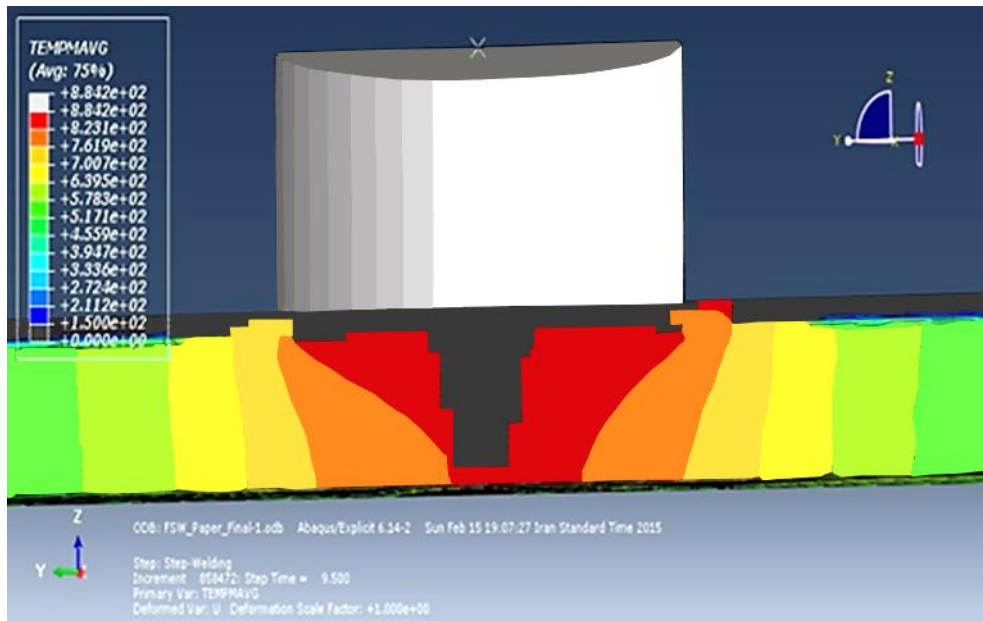
Fig. 8 - Effects of rotational speed on the HAZ width for the two aluminum alloys.

## 4-2 Effects of traverse speed

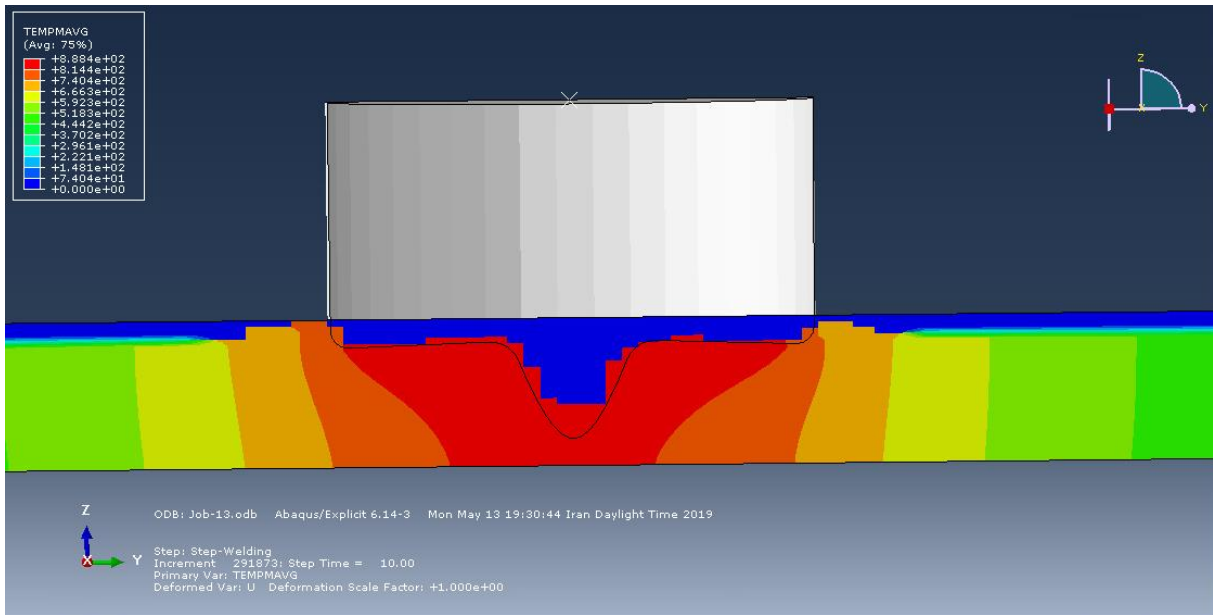
Figure 9 illustrates the temperature fields across the welding zone for different traverse speeds revealing that an increase in the traverse speed produces a decrease in temperature within the material. In fact, increasing the traverse speed leads to lower strain rates and friction decreasing directly the heat input into the weld joint. Figure 9(A) indicates the maximum operating temperature of 909 K obtained at the minimum traverse speed of 1.5 mm/s which is the slowest value used in this study. Figure 10 presents the evolution of weld width according to the traverse speed for the two aluminum alloys where an increase in traverse speed produces a decrease in weld width for AA6061-T6. The simulation results also confirmed that the weld widths obtained with AA6061-T6 are generally larger than those obtained with AA5083-O irrespectively to the traverse speeds. Figure 11 illustrates the effects of traverse speed on the weld depth for the two aluminum alloys. Figure 12 indicates the effects of traverse speed on HAZ width for the two aluminum alloys where the zones affected by heat of the AA6061-T6 seem to be larger than that obtained for AA5083-O for all traverse speeds as a result of higher thermal conductivity of the AA6061-T6 and higher specific heat of the AA5083-O.



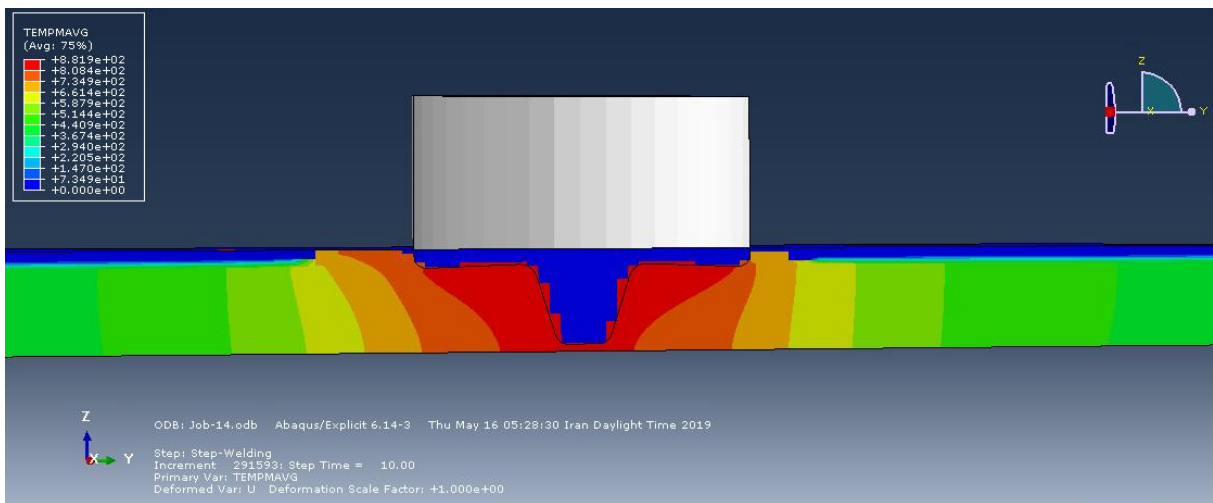
(A)



(B)



(C)



(D)

**Fig 9. Effects of traverse speed on the weld width, HAZ width, and weld depth for traverse speeds of A) 1.5 mm/s, B) 2.5 mm/s, C) 3.5 mm/s, and D) 4.5 mm/s**

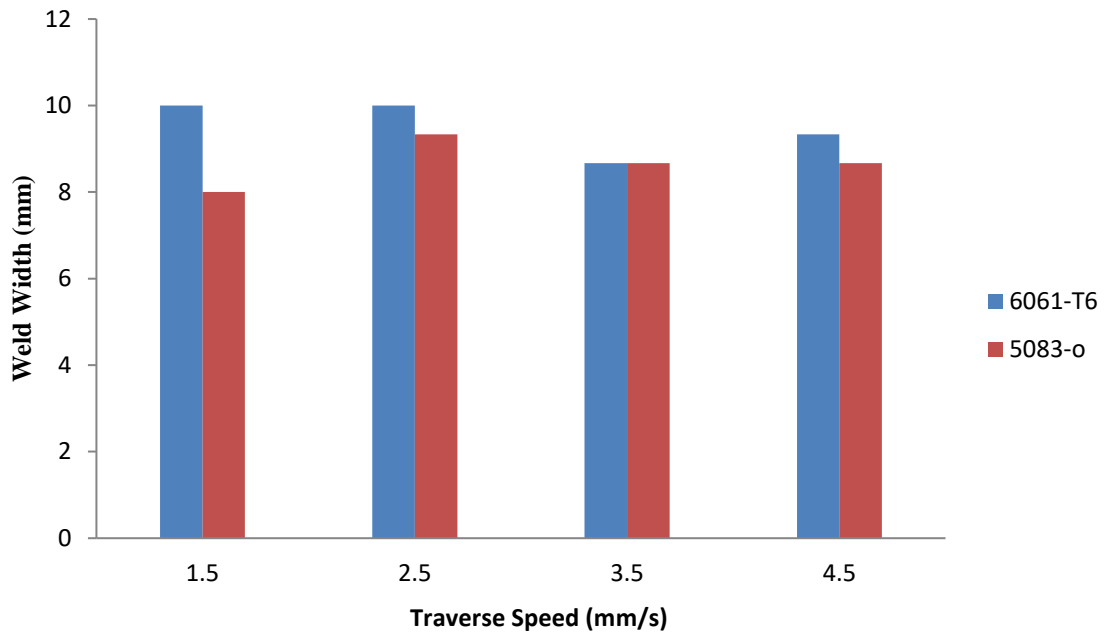


**Fig. 10** Effects of traverse speed on the weld width for the two aluminum alloys.

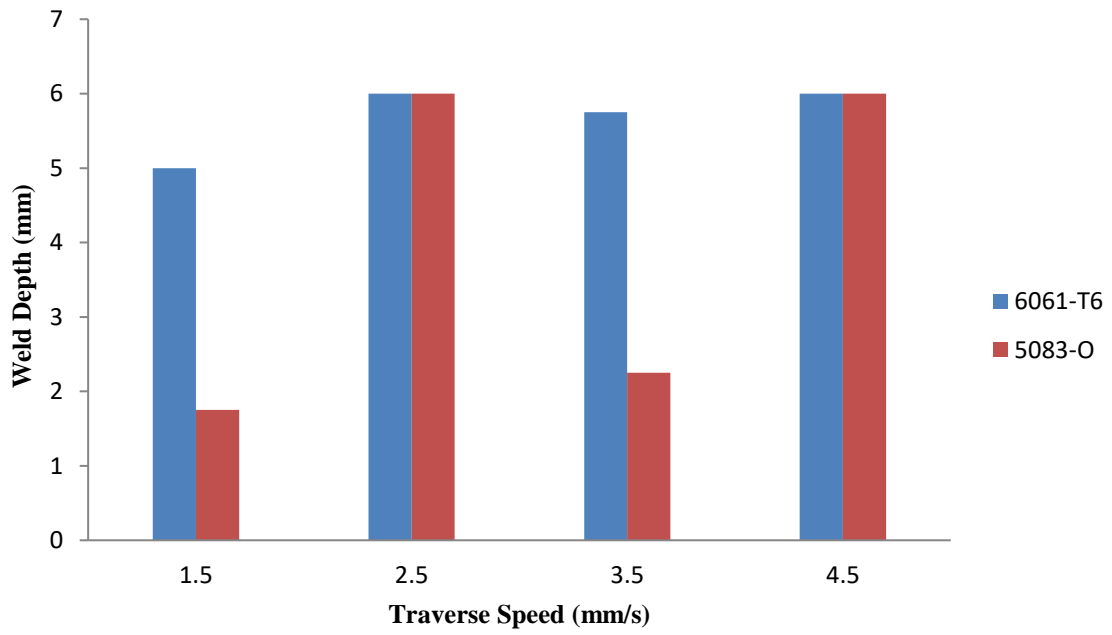
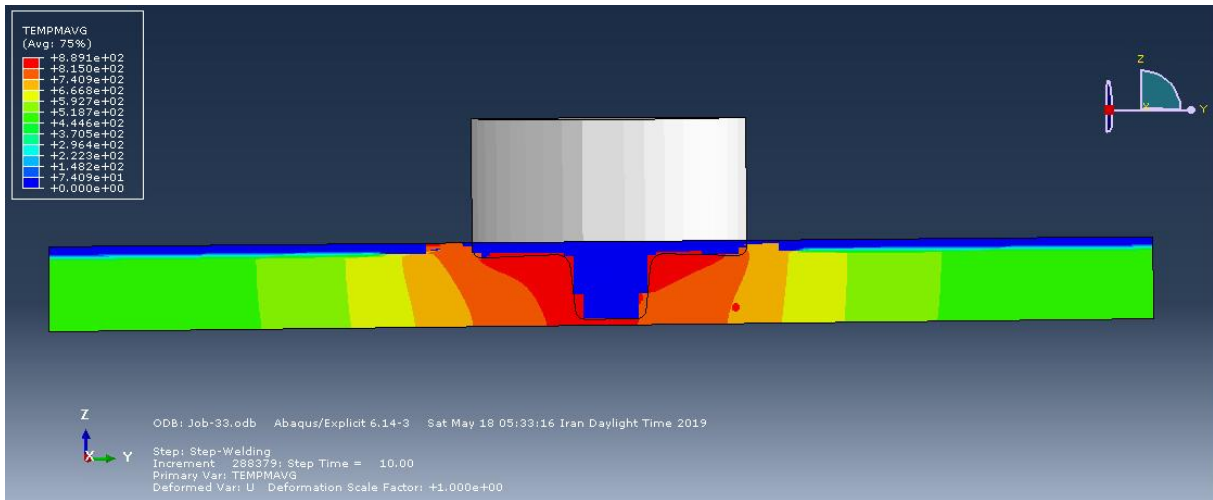
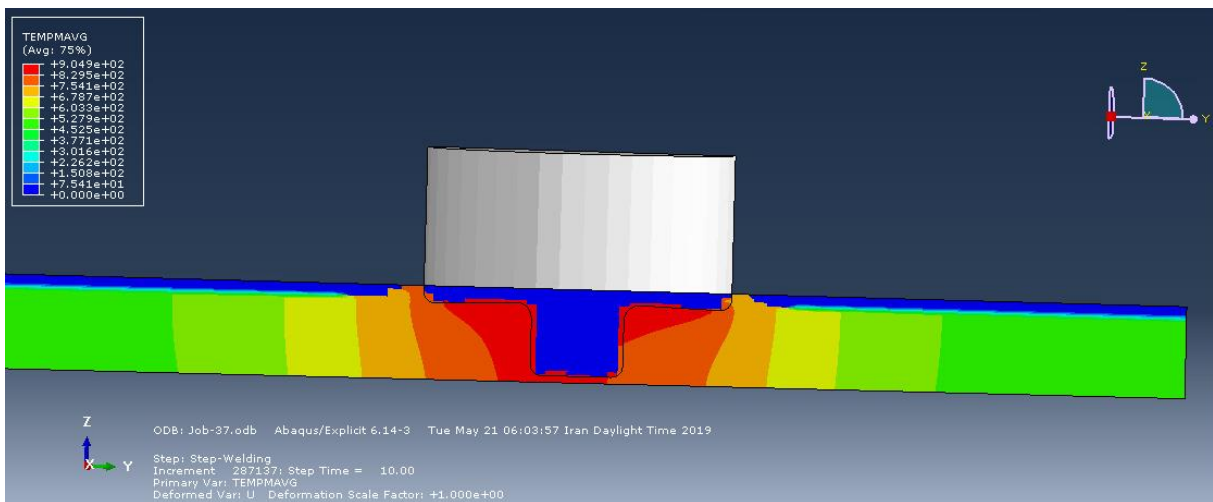


**Fig. 11** - Effects of traverse speed on the weld depth for the two aluminum alloys.

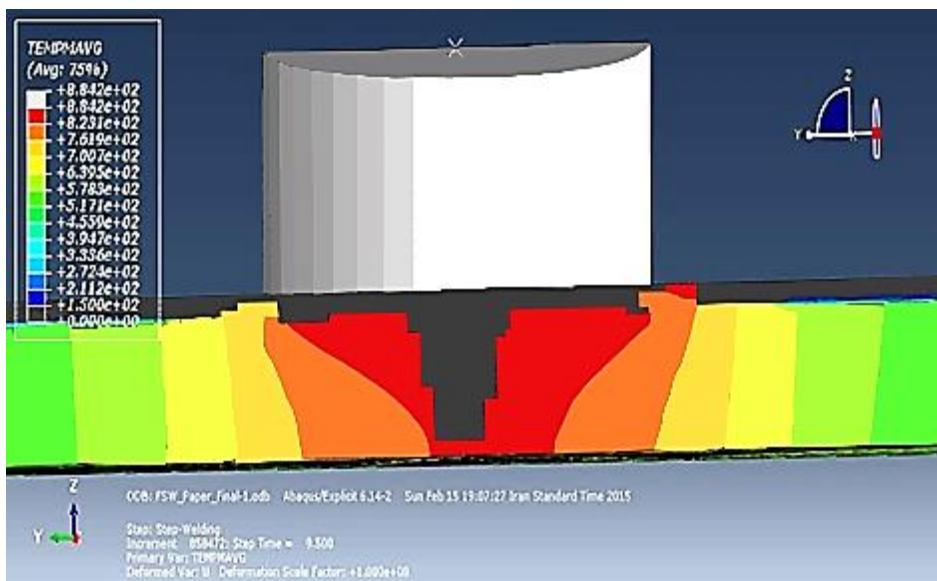




(B)



(C)



(D)

**Fig 13. Effects of tool diameter on the weld width, HAZ width, and weld depth for tool diameters of A) 2 mm, B) 2.5 mm, C) 3 mm, and D) 3.5 mm**

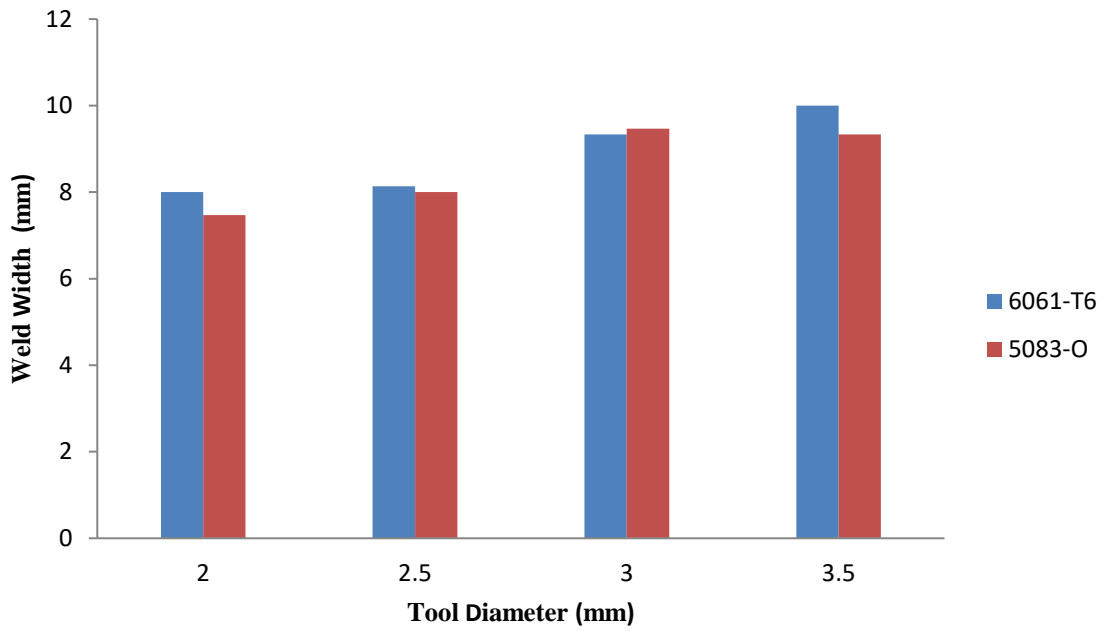


**Fig. 14 - Effects of tool diameter on the weld width for the two aluminum alloys.**

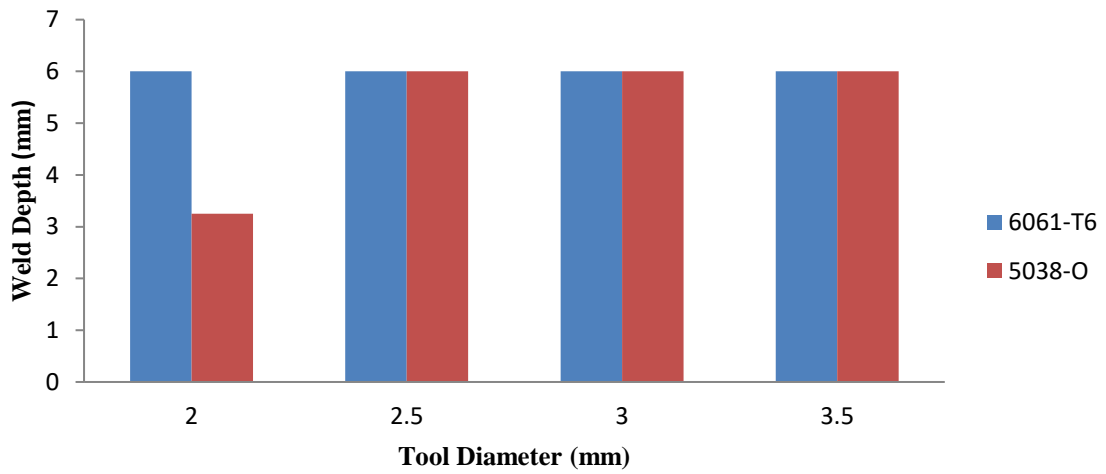


**Fig. 15 - Effects of tool diameter on the weld depth for the two aluminum alloys.**

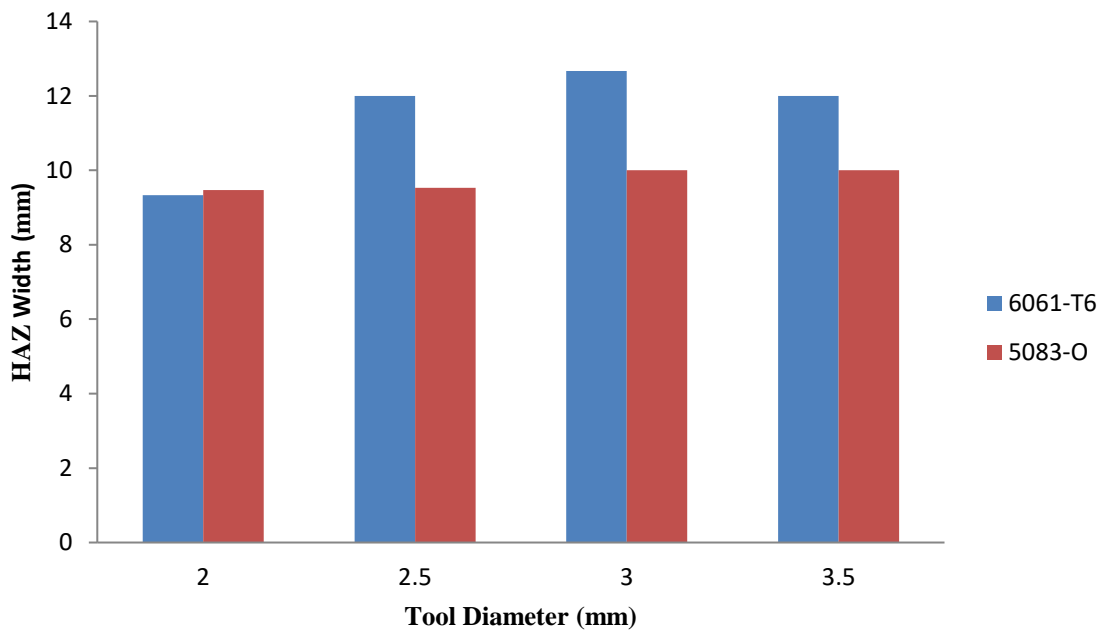


Fig. 16 - Effects of tool diameter on the HAZ width for the two aluminum alloys.

## 5- Conclusions

In the current study friction stir welding of two aluminum alloys (AA 5083-0 and AA 6061-T6) are investigated using numerical analysis. The following conclusions are listed:

- The welding process parameters have direct effects on temperature distribution in the materials and maximum operating temperature of about 900 K in almost all cases are lower than the minimum melting temperature of the aluminum alloys.
- Temperature of the base materials is increased when the rotational speed and traverse speed are increased and decreased, respectively.
- As the rotational speed of the tool increases, the weld widths are reduced. Full penetration is seen for both aluminum alloys at all rotational speeds except for AA5083-O at a speed of 740 rpm.
- Increasing traverse speed slightly changes the weld width and HAZ width of the AA5083-O.
- Increasing the diameter of the tool generally results in a larger contact area increasing the weld width in both alloys. However, the HAZ width for AA5083-O is sensitive to the tool diameter.
- The HAZ width for AA6061-T6 is larger than that of AA5083-O for almost all welding conditions due to the intrinsic properties of AA6061-T6 (higher thermal conductivity and lower specific heat).

## References

1. D. Rao, K. Huber, J. Heerens, J. F. dos Santos, and N. Huber, 2013, Asymmetric mechanical properties and tensile behaviour prediction of aluminium alloy 5083 friction stir welding joints, *Materials Science and Engineering: A*, 565, pp. 44–50.
2. R. S. Mishra, P. S. De and N. Kumar, 2014, *Friction Stir Welding and Processing: Science and Engineering*, Springer International Publishing Switzerland.

3. R. Gabor, A. Roos, J. dos Santos, L. Bergmann, 2009, Friction Stir Welding of AA 5083-H111 Alloy, International Conference on Innovative technologies for joining advanced materials, pp. 51–56.
4. M.A. Trishul, H. Virupaxayya, P. Shreyas, 2015, Production and testing of Al-Fe<sub>2</sub>O<sub>3</sub> particulate composite, International Advanced Research Journal in Science, Engineering and Technology, 2(4), pp. 19-24. DOI: 10.17148/IARJSET.2015.2405
5. K. Elangovan and V. Balasubramanian, 2007, Influences of pin profile and rotational speed of the tool on the formation of friction stir processing zone in AA2219 aluminium alloy, Material Science and Engineering: A, 459(1-2), pp. 7-18.
6. Y.G. Kim, H. Fujii, T. Tsumura, T. Komazaki and K. Nakata, 2006, Three defect types in friction stir welding of aluminum die casting alloy, Material Science and Engineering: A, 415(1-2), pp. 250-254.
7. R.S. Mishra and Z.Y. Ma, 2005, Friction stir welding and processing, Materials Science and Engineering: R: Reports, 50(1-2), pp.1-78
8. W. M. Thomas and E. D. Nicholas, 1997, Friction stir welding for the transportation industries, Materials & Design, 18(4-6), pp. 269-273.
9. H. Raikoty, I. Ahmed, G.E. Talia, 2005, High speed friction stir welding: A computational and experimental study, Proceedings of the ASME Summer Heat Transfer Conference, pp. 431-436.
10. A.H. Jamshidi, S. Serajzadeh, A.H. Kokabi, 2011, Evolution of microstructures and mechanical properties in similar and dissimilar friction stir welding of AA5086 and AA6061, Material Science and Engineering: A, 528(28), pp. 8071–8083.
11. L. Dubourg, A. Merati, M. Jahazi, 2010, Process optimisation and mechanical properties of friction stir lap welds of 7075-T6 stringers on 2024-T3 skin, Materials & Design, 31(7), pp. 3324–3330.
12. N.T. Kumbhar, S.K. Sahoo, I. Samajdar, G.K. Dey, K. Bhanumurthy, 2011, Microstructure and microtextural studies of friction stir welded aluminium alloy 5052, Materials & Design, 32(3), pp. 1657-1666.
13. S.D. Ji, Q.Y. Shi, L.G. Zhang, A.L. Zou, S.S. Gao, L.V. Zan, 2012, Numerical simulation of material flow behavior of friction stir welding influenced by rotational tool geometry, Computational Materials Science, 63, pp. 218–226.
14. P. Sadeesh, K.M. Venkatesh, V. Rajkumar, P. Avinash, N. Arivazhagan, R. Devendranath, S. Narayanan, 2014, Studies on friction stir welding of AA 2024 and AA 6061 dissimilar metals, Procedia Engineering, 75, pp. 145 – 149
15. R. K. Kesharwania, S. K. Pandab, S. K. Palc, 2014, Multi Objective Optimization of Friction Stir Welding Parameters for Joining of Two Dissimilar Thin Aluminum Sheets, Procedia Materials Science, 6 , pp. 178 – 187
16. J.H. Choa, W. J. Kima, C. G. Leea, 2014, Evolution of microstructure and mechanical properties during friction stir welding of A5083 and A6082, Procedia Engineering, 81, pp. 2080 – 2085.
17. N. Dialami, M. Cervera, M. Chiumenti, C. Agelet de Saracibar, 2017, Local–global strategy for the prediction of residual stresses in FSW processes, The International Journal of Advanced Manufacturing Technology, 88(9–12), pp. 3099–3111
18. M. Iordache, C Badulescu, D Iacomi, E Nitu, C. Ciuca, Numerical Simulation of the Friction Stir Welding Process Using Coupled Eulerian Lagrangian Method, 2016, ModTech International Conference - Modern Technologies in Industrial Engineering IV, 145, 022017
19. R. M. F. Paulo<sup>1</sup>, P. Carlone, R. A. F. Valente, F. Teixeira-Dias, G. S. Palazzo, 2016, Numerical simulation of friction stir welding (FSW): Prediction of the heat affect zone using a softening model, AIP Conference Proceedings, 1769, 060011
20. M. Kim, J. S. Kim, 2017, Numerical Simulation of Friction Stir Welding of Magnesium Alloy considering Fluid Dynamics, Proceedings of the 4<sup>th</sup> International Conference of Fluid Flow, Heat and Mass Transfer (FFHMT'17)
21. G. Chen, H. Li, G. Wang, Z. Guo, S. Zhang, Q. Dai, X. Wang, G. Zhang, Q. Shia, 2018, Effects of pin thread on the in-process material flow behavior during friction stir welding: A computational fluid dynamics study, International Journal of Machine Tools and Manufacture, 124, pp. 12-21

22. M.I. Costa, C. Leitão, D.M. Rodrigues, 2019, Parametric study of friction stir welding induced distortion in thin aluminum alloy plates: A coupled numerical and experimental analysis, *Thin-Walled Structures*, 134, pp. 268–276
23. B. Meyghani, M. B. Awang, S. S. Emamian, M. K. B. Mohd Nor, S. R. Pedapati, 2017, A Comparison of Different Finite Element Methods in the Thermal Analysis of Friction Stir Welding (FSW), *Metals*, 7(10), 450; <https://doi.org/10.3390/met7100450>
24. N. Dialami, M. Chiumenti, M. Cervera, C. Agelet de Saracibar, 2017, Challenges in Thermo-mechanical Analysis of Friction Stir Welding Processes, *Archives of Computational Methods in Engineering*, 24(1), pp. 189–225
25. F. Al-Badour, N. Merah, A. Shuaib, A. Bazoune, 2014, Thermo-mechanical finite element model of friction stir welding of dissimilar alloys, *The International Journal of Advanced Manufacturing Technology*, 72(5-8), pp. 607-617
26. M.M. El-Sayed, A.Y. Shash, M. Abd-Rabou, 2018, Finite element modeling of aluminum alloy AA5083-O friction stir welding process, *Journal of Materials Processing Tech*, 252, pp. 13–24
27. M. Riahi and H. Nazari, 2011, Analysis of transient temperature and residual thermal stresses in friction stir welding of aluminum alloy 6061-T6 via numerical simulation, *The International Journal of Advanced Manufacturing Technology*, 55(1-4), pp. 143–152.
28. M.M. El-Sayed, A.Y. Shash, T.S. Mahmoud, M.A. Rabbou, 2018, Effect of Friction Stir Welding Parameters on the Peak Temperature and the Mechanical Properties of Aluminum Alloy 5083-O, *Advanced Structured Materials*, 72, pp. 11-25.
29. Z. Zhu, M. Wang, H. Zhang, X. Zhang, T. Yu, Z. Wu, 2017, A Finite Element Model to Simulate Defect Formation during Friction Stir Welding, *Metals*, 7(7), 256; <https://doi.org/10.3390/met7070256>
30. Y. Zhang, J.C. Outeiro, T. Mabrouki, 2015, On the selection of Johnson-Cook constitutive model parameters for Ti-6Al-4V using three types of numerical models of orthogonal cutting, *Procedia CIRP*, 31, pp. 112 – 117.
31. V. Năstăsescu and N. Iliescu, 2010, Upon accompanying of the experimental testing of materials by numerical analysis with FEM, *Acta Technica Napocensis - Series: Applied Mathematics and Mechanics*, 2(53), pp. 173-178.
32. M. Grazka and J. Janiszewski, 2012, Identification of Johnson-Cook Equation Constants using Finite Element Method, *Engineering Transactions*, 60(3), pp. 215–223.
33. B. Meyghani, M. Awang, S. Emamian, Nor M. Khalid, 2017, Developing a Finite Element Model for Thermal Analysis of Friction Stir Welding by Calculating Temperature Dependent Friction Coefficient, *2nd International Conference on Mechanical, Manufacturing and Process Plant Engineering*, pp 107-126